Advances in Water Resources 131 (2019) 103385

Contents lists available at ScienceDirect

Advances in Water Resources

journal homepage: www.elsevier.com/locate/advwatres

Contribution of the main moisture sources to precipitation during extreme peak precipitation months

Raquel Nieto[a,*], Danica Ciric[a], Marta Vázquez[a,b,c], Margarida L.R. Liberato[b,c], Luis Gimeno[a]

[a] Environmental Physics Laboratory (EPhysLab), CIM-UVIGO, Universidad de Vigo, Ourense 32004, Spain
[b] Instituto Dom Luiz, Universidade de Lisboa, 1749-016 Lisboa, Portugal
[c] Escola de Ciências e Tecnologia, Universidade de Trás-os-Montes e Alto Douro, Vila Real, Portugal

ARTICLE INFO

Keywords:
Contribution to precipitation
Lagrangian modelling
Extreme precipitation
Sources of moisture

ABSTRACT

A worldwide study is presented to understand the role of major global moisture source regions in the occurrence of extreme monthly precipitation over the continents. The Lagrangian model FLEXPART v9.0 was used to analyse the moisture transport for precipitation, and the extreme precipitation was calculated for each grid point (at 0.25°) using the Multi-Source Weighted-Ensemble Precipitation (MSWEP) monthly precipitation dataset. Although the eventual aim of this work is to show the link between the contributions from the sources to their sinks during months of extreme rainfall, we provide, for the first time, much-needed information on these contributions at a monthly scale – previously this information was only available at an annual scale. We also provide maps showing global monthly moisture sources, together with the identification of the peak precipitation month (PPM) and of the preferred moisture source for precipitation in that month.

1. Introduction

A primary concern related to climate change is not just the variation in the mean variables of climate, but also in their extremes (Santos and Costa, 2014). Several authors have pointed to future increases in the frequency and magnitude of extremes (Smith, 2011; Singh et al., 2013; Fischer et al., 2013). Understanding how climate change affects these extremes is important due to their impact on the environment and on society as a whole (e.g., Frank et al., 2015; Butt et al., 2015; Nolet and Kneeshaw, 2018; O'Lenick et al., 2019). Such understanding is also crucial monitoring and preparedness of unexpected extreme events (Toreti and Desiato, 2008). Under a warmer climate, precipitation will change substantially (Trenberth, 2011) and the frequency of extreme wet and dry years is expected to increase (Knapp et al., 2015; Ramos et al., 2016). Extreme precipitation events lead to major natural disasters around the world and are the main cause of flood events. Because of this, the comprehensive analysis of global precipitation climatology and the assessment of extreme precipitation events are of particular interest.

To better understand the likely impacts of global climate change on the water cycle, the link between oceanic and terrestrial sources and precipitation is especially relevant (e.g., Gimeno et al., 2010; van der Ent and Savenije, 2013). The identification of the major sources of precipitation is thus important for areas where there are changes in the hydrological cycle due to climate change (Gimeno et al., 2013). Given the importance of this topic, previous authors have investigated the major oceanic and terrestrial water sources of precipitation and their corresponding sink regions at a global (Gimeno et al., 2010; van der Ent et al., 2010) and a regional scale (e.g., Drumond et al., 2014; Sodemann and Zubler, 2010). Gimeno et al. (2010) and Castillo et al. (2014) analysed the oceanic moisture sources using the maximum values of annual divergence flux of moisture. They observed an asymmetrical influence of moisture source regions on precipitation over land in terms of both extent and importance. While the moisture contribution from some large oceanic sources, for instance the South Pacific Ocean, is localized over large continental areas, some smaller sources provide moisture to widespread, vast areas in proportion to their sizes. For example, the Black Sea provides moisture for precipitation over Central Europe (Ciric et al., 2016), the Arabian Peninsula (Heydarizad et al., 2018), and even the Arctic region (Vázquez et al., 2016). Moreover, despite some continental regions receiving moisture from several sources, other regions have no moisture contribution for precipitation from any of these major moisture sources, as identified by Gimeno et al. (2010) and Castillo et al. (2014), where the moisture contribution is more local (e.g.: Greenland Sodemann et al., 2008 or inland parts of Asia Sato et al., 2007). Further details of the main sources of moisture and their contribution to precipitation over continental areas can be found in Gimeno et al. (2010,2013).

In the present work, the analysis of Gimeno et al. (2010) and Castillo et al. (2014) is revisited in order to allow identification of the major oceanic and terrestrial sources of extreme precipitation for the

* Corresponding author.
E-mail address: rnieto@uvigo.es (R. Nieto).

https://doi.org/10.1016/j.advwatres.2019.103385
Received 30 January 2019; Received in revised form 25 July 2019; Accepted 1 August 2019
Available online 3 August 2019

whole of the period 1980–2015. From the detection of these moisture sources, a complete collection of maps of precipitation is developed, taking into account only monthly extremes of precipitation. The aim of this work is twofold, (i) to collate maps of global extremes, and (ii) enhance understanding of the role of the major sources of moisture (oceanic and continental) during the months with intense precipitation. Monthly data from the Multi-Source Weighted-Ensemble Precipitation (MSWEP) dataset are used to analyse the precipitation extremes, and the outputs from the FLEXible PARTicle dispersion (FLEXPART) model are used to compute the associated moisture transport.

2. Methodology

2.1. Moisture source region definition

Identification of the major global moisture source regions is based on the methodology established by Gimeno et al. (2010). The method uses the Vertically Integrated Moisture Flux (VIMF) divergence to localize maximum values, which are associated with evaporative areas. Using VIMF data obtained from the ERA-Interim dataset (Dee et al., 2011) at a $1^\circ \times 1^\circ$ horizontal resolution, the climatological flux divergence was computed for each month individually over a 36-year period, 1980–2015.

Gimeno et al. (2010) imposed fixed annual thresholds of 750 and 500 mm/year to identify the oceanic and continental moisture sources (the fiftieth and fortieth percentiles, respectively). Here, the thresholds are imposed monthly and the moisture sources are defined as those areas showing values higher than the threshold for each month.

2.2. Continental sink regions and FLEXPART methodology

In order to analyse the regions affected by each of the detected sources and to assess how much moisture is provided to these areas, the Lagrangian particle dispersion model FLEXPART is applied. This model was developed by Stohl (1999) and is widely used to analyse moisture transport (e.g., Sodemann et al., 2008; Nieto et al., 2010; Vázquez et al., 2016; Sorí et al., 2017). The input data for running FLEXPART is ERA-Interim reanalysis at a resolution of 1° x 1° degrees in latitude and longitude and on native ECMWF (European Centre for Medium Range Weather Forecasting) model levels. FLEXPART uses 3D wind to transport and move the particles and, among other parametrization, turbulent dispersion is handled by a subroutine that calls procedures to interpolate winds (a complete model configuration can be found in Stohl and James, 2005). Therefore, the final trajectories (outputs) need not be in the initial grid (1° x 1°), and the changes in any variable over a particular area can be calculated for the grid required by the user (with a number of air particles that must be higher than the ECMWF model levels).

FLEXPART is used for a global experiment in which about 2 million air particles are released every 6 h (with intermediate data added every 3 h (Stohl and James, 2004)). Outputs were used to analyse changes in moisture experienced by the particles along their trajectories. In the present work, changes in specific humidity are used to analyse the moisture contribution from the major sources over the continents. However, there are many different parameters that may influence the variability of the precipitation (Xue et al., 2017; Tandon et al., 2018); for example, the influence of temperature on extreme precipitation is well known (Westra et al., 2013; Hoerling et al., 2016). Although the direct effect of temperature is not investigated in the present study, a discussion of the influence of this and other parameters on the hydrological cycle was provided by Gimeno et al. (2012).

The approach used here is based on the methodology established by Stohl and James (2004, 2005). To investigate the sink regions for a particular source, the model follows the particles that leave the source forwards in time (Stohl and James, 2004, 2005) for a limited transport time of 10 days (the average time spent by water vapour in the atmosphere as indicated by Numaguti, 1999, and corroborated by van der Ent and Tuinenburg, 2017 and Nieto and Gimeno, 2019) – the so-called forward tracking mode or forward methodology. Along each trajectory, the programme stores the specific humidity together with the position (latitude, longitude and altitude) of each particle at 6 h time step (00, 06, 12 and 18 UTC). By calculating the changes in specific humidity (q) at each time step, the variations in moisture given the evaporation (e) and precipitation (p) experienced by the particles can be identified by the equation $(e-p) = m(dq/dt)$, where m indicates the mass of the particle and dt indicates the 6-h time interval. Considering all (e-p) values of the particles in an atmospheric column over a target region for an area A, it is possible to calculate the total surface freshwater flux as

$$(E - P) \approx \frac{\sum_{k=1}^{k=K} (e-p)_k}{A} \quad (1)$$

where k is the number of particles considered.

To identify the sinks of moisture, the regions where the total precipitation (P) exceeds the total evaporation (E) should be selected, so only those regions showing $(E-P) < 0$ values are taken into account at a resolution of 0.25° x 0.25° degrees.

2.3. Precipitation analysis

To describe characteristics of global precipitation in terms of annual and monthly precipitation climatology, the MSWEP database (Beck et al., 2017) is used. The MSWEP database covers the period from 1980–2015, and is available at a spatial resolution of $0.25^\circ \times 0.25^\circ$ latitude and longitude. Available since 2017, this dataset combines the advantages of a wide range of data sources (eg., from reanalyses as the Japanese 55-year Reanalysis (JRA-55) and ERA-Interim, and from estimation on gauges as Global Historical Climatology Network-Daily (GHCN-D), WorldClim, Global Precipitation Climatology Centre (GPCC) or Global Summary of the Day (GSOD), and from satellites as the Gridded Satellite (GridSat), Climate Prediction Center morphing technique (CMORPH), Tropical Rainfall Measuring Mission (TRMM) Multisatellite Precipitation Analysis (TMPA) 3B42RT, and Global Satellite Mapping of Precipitation (GSMaP)) to provide reliable precipitation estimates around the world.

From this dataset, the Peak Precipitation Month (PPM) is defined as that containing the maximum precipitation for each grid point for the whole period. The mean precipitation (calculated from MSWEP) in that PPM for each grid point is calculated and herein denoted as PMSWEP. This value allows assessing extreme monthly precipitation for each grid point.

2.4. Preferred Source and moisture source contribution for the PPM

The Preferred Source (PS) of moisture is defined as the source providing most of the moisture for precipitation to each grid point in the PPM. In order to identify the PS, the total contribution from each individual moisture source is computed following the particles trajectories simulated by FLEXPART dispersion model with the forward in time methodology (Stohl et al., 2005). Therefore, the source that shows the highest values of $|(E-P) < 0|$ (measured in mm/day) is the PS for the corresponding grid point. The values of $|(E-P) < 0|$ associated only with the PS for the PPM are denoted herein as PFLEX-PS. The moisture contribution is also analysed taking into account all the sources (not only the PS) that show some contribution at each grid point. In this case, the values of $|(E-P) < 0|$ from all sources (not just the PS) are included; this field is denoted PFLEX.

3. Results and discussion

3.1. Characterization of global monthly moisture sources and sinks

To investigate the monthly role of the major moisture sources for the peak precipitation months (PPMs) for each 0.25° grid point, it is first

Table 1
Monthly values for oceanic (fiftieth percentile) and continental (fortieth percentile) sources.

Month	Oceanic sources (p50) mm/year	Land sources (p40) mm/year
January	830.8	498.3
February	768.4	496.8
March	699.9	447.7
April	656.3	466.9
May	670.4	440.7
June	838.3	474.1
July	849.6	477.5
August	748.3	489.5
September	659.2	447.9
October	721.3	501.0
November	768.7	508.4
December	807.4	480.8

necessary to identify moisture sources and the corresponding sinks. The first part is achieved following the methodology of Gimeno et al. (2010), as described in the methodology section. The fiftieth (p50) and fortieth (p40) percentiles are applied to the VIMF divergence to define oceanic and continental sources, respectively. In the present work, the threshold values of VIMF divergence differ from month to month and between oceanic and continental sources. The data contained in Table 1 confirm that the threshold values vary between 656 and 850 mm/year for oceanic and 440–508 mm/year for terrestrial sources, which are within the approximate range of values used in Gimeno et al. (2010).

A total of 14 moisture sources were identified. Eleven are oceanic, namely NPAC (North Pacific), SPAC (South Pacific), MEXCAR (Gulf of Mexico and Caribbean Sea), NATL (North Atlantic), SATL (South Atlantic), ZANAR (Zanzibar Current and Arabian Sea), AGU (Agulhas Current), IND (Indian Ocean), CORALS (Coral Sea), MED (Mediterranean Sea), and REDS (Red Sea). Three are continental: SAM (South America), SAHEL (Sahel region), and SAFR (South Africa). Because MED and RED occupy almost the whole of the area inside their basins, these two sources are defined using their physical boundaries. The left-side panels of Fig. 1 show oceanic and terrestrial moisture source regions for January and July (mid-boreal winter and mid-boreal summer months). Figures for all months can be found in the Supplementary Material (Figs. A.1–A.12). At global scale, most of the detected moisture sources are located over tropical and subtropical oceanic areas, including the continental areas of South America, South Africa, and the Sahel region.

The areas of contribution of the detected sources to continental precipitation are estimated using the forward tracking mode in the outputs of the Lagrangian dispersion model FLEXPART (Stohl et al., 2005) for the period 1980–2015. This calculation is performed for each month, but for simplicity the results and explanation are presented here only for January and July (Fig. 1, right-side panels). Similarly, the results for all months can be found in the Supplementary Material (Figs. A.1–A.12). For each month, the continental sink regions for the oceanic sources (top right) and for the continental sources (bottom right) are presented separately. Each colour used in the figures for the sinks is associated with the same colour in the figure for the moisture sources in the left-hand panels. Thus, for instance, areas in red over South America and the coast of Africa in January (a, top-right figure) represent sink regions for the SATL source (red in the top-left figure).

In general, the moisture sources identified at a monthly scale are quite similar to those found by Gimeno et al. (2010) and Castillo et al. (2014) in terms of their location and extent. However, it is interesting to note that the moisture sources are not stationary. They show differences in intensity between months, which is reflected in their spatial extents and thus the associated sinks.

The selection of thresholds is always a source of uncertainty. In this study, the limits imposed are large enough to comprise the maximum values of VIMF, where the major monthly global evaporation occurs. The oceanic moisture taken into account using these thresholds include vast areas that extend from one side of the ocean to the other, with the coasts acting as geographical barriers in many cases (see Gimeno et al., 2010 or Castillo et al., 2014). If different thresholds were to be applied, the latitude would be the only dimension to show a slight growth. In any case, if the area of the moisture source was bigger, there would be a few more particles to be forward tracked, and no perceptible difference would be noted in the final computation of E-P<0 over each grid point.

In terms of annual variability, some sources are present throughout the year, while others are greatly reduced or completely absent in some months. For example, in both the northern and southern hemispheres, the PAC and ATL sources are present during both January and July, and also during all other months (see Supplementary Material Figs. A.1–A.12). ZANAR (in the northern hemisphere) and IND (in the southern hemisphere) also provide moisture throughout all the year. On the other hand, some sources vary throughout the year. For example CORALS; while the source practically disappears in January, it is strong in July. MEXCAR (the Mexico Caribbean source) shows another example of this behaviour. From January to April, this source shows its maximum extent, but it weakens from May until August, before disappearing altogether in September. From October, it appears again as an important moisture source (for the complete annual evolution see Supplementary Material Figs. A.1–A.12). Similar patterns are also observed for the continental sources of SAM, SAFR, and SAHEL. Fig. 1 shows that in January the SAHEL is the only moisture source on land, but it disappears during July, when SAFR and SAM appear. The SAHEL source exhibits a clear seasonal dichotomy; during late spring and summer (April-September) it is absent, while during the extended winter (October-March) it is an important source. SAM is a bigger moisture source between April and October but it is greatly reduced in September and October, appearing only over the north-eastern part of Brazil.

The sinks of moisture associated with each source in Fig. 1 (right-side panels, and in the corresponding Supplementary Material Figs. A.1–A.12) show that oceanic subtropical areas dominate as moisture providers (as in Gimeno et al., 2010). Thus, the North Atlantic Ocean (NATL) is the dominant moisture source during January, providing moisture for precipitation in three continents: Europe, Eastern North America, and South America. In July, its influence is weakened, and it contributes to only small parts of Mexico, Central America, and Northern South America. On the other hand, the South Atlantic Ocean (SATL) contributes to precipitation during January and July, mainly providing the moisture for Brazil and Central Africa.

There is no rule that the major moisture sources necessarily provide precipitation to huge continental areas as demonstrated by the Indian and South Pacific Oceans during both January and July. In contrast, there are some small moisture source regions that provide large amounts of moisture for precipitation in comparison with their size. For example, the Mediterranean Sea is an important water source for Europe and North Africa throughout the year. In particular, the Mediterranean Sea represents the only source (from those identified here) that contributes to Northern Africa (throughout the year) and to some areas of Europe (especially in summer). Another example is the Red Sea, which provides great quantities of precipitation for the whole coast of the Middle East (including parts of Syria, Iraq, and Iran) from January to April. This points to the importance of the source in the hydrological cycle for these continental areas.

During January, MEXCAR is the dominant moisture source for precipitation over Europe and Eastern North America, extending its influence across the Northern American continent in July, although with reduced intensity.

On the other hand, there are also some areas, for example Australia and Canada, which generally receive precipitation from a single source throughout the year. The dominant moisture source for Australia is CORALS (Coral Sea) during both January and July, while for Canada it is the North Pacific Ocean (NPAC).

Continental moisture sources are important providers of precipitation in those months when they appear to be the most significant

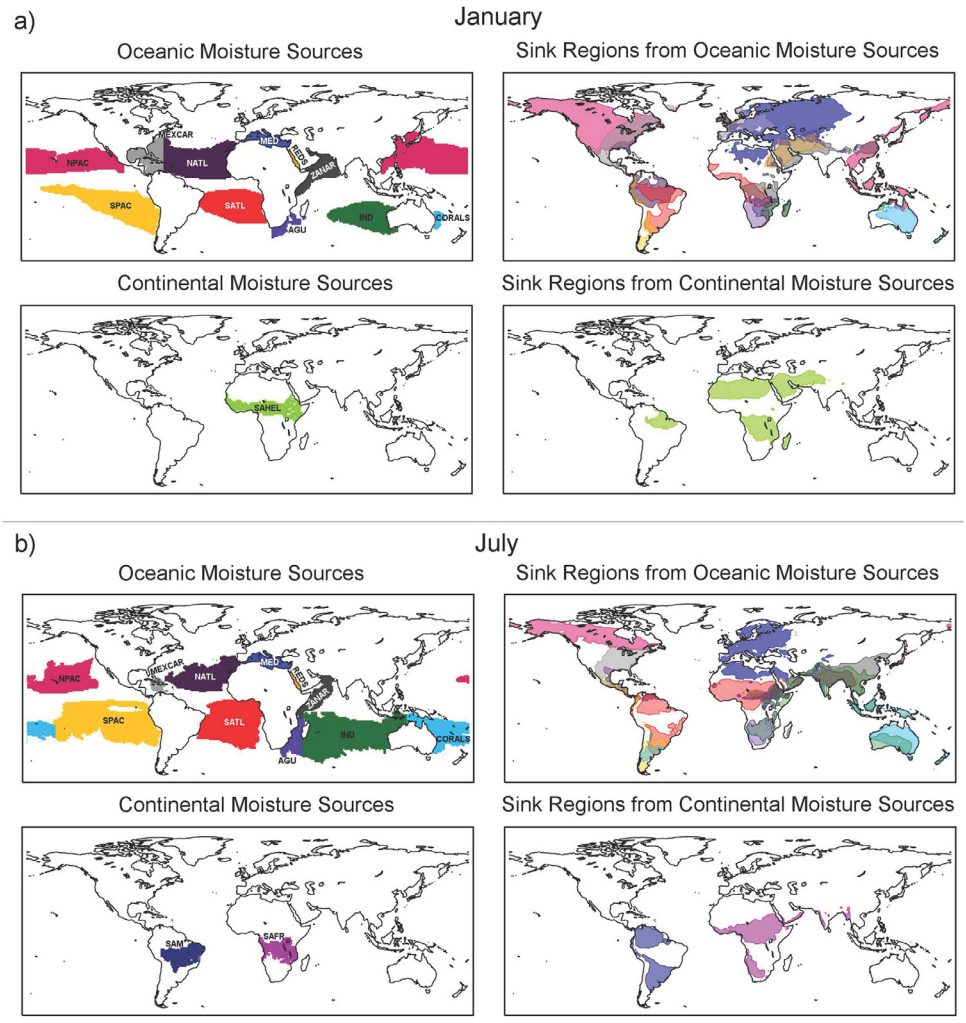

Fig. 1. Schematic representation of oceanic and continental moisture sources and their associated sinks calculated for the period 1980–2015 for January (a) and July (b). Left panels: The thresholds used to identify oceanic sources were 830.8 mm/day for January (a, top-left figure) and 849.6 mm/day for July (b, top-left figure). Both values represent the 50th percentile of the monthly VIMF divergence. The sources identified for both months are as follows: NPAC, North Pacific; SPAC, South Pacific; MEXCAR, Mexico Caribbean; NATL, North Atlantic; SATL, South Atlantic; MED, Mediterranean Sea; REDS, Red Sea; ZANAR, Zanzibar Current; AGU, Agulhas Current; IND, Indian Ocean an CORALS, Coral Sea (as in Gimeno et al. (2010) and Castillo et al. (2014)). Continental moisture sources were calculated using the 40th percentile of the monthly VIMF divergence, the threshold being 498.3 and 477.5 mm/day for January (a, bottom-left figure) and July (b, bottom-left figure) respectively. Continental moisture sources identified are SAHEL (Sahel region) for January, and SAM (South America) and SAFR (South Africa) for July. The right-hand panels show the sink regions over the continents (E - P < 0 values) identified from a FLEXPART forward particle tracking of those air masses leaving each source of moisture. They are plotted for values lower than −0.05 mm/day. The colour of each is the same as that of the related source in the left-hand panels, and any overlap of sinks is shown using a darker shading. (For interpretation of the references to color in this figure, the reader is referred to the web version of this article.)

moisture source regions. For instance, in January, the Sahel region provides precipitation for vast continental areas including parts of North and South Africa, the coast of the Middle East, and the north-eastern part of Brazil. During July, SAM and SAFR are important moisture sources for precipitation for South America and Central and Southern Africa, respectively.

This source-sink relationship is in agreement with previous results. For example, the North Atlantic Ocean and the Mediterranean Sea have previously been identified as major sources for Europe (Nieto et al., 2010), and the South Pacific Ocean was previously found to provide most of the moisture arriving in Central Brazil and the La Plata Basin (Drumond et al., 2008). The monthly variability of the contribution of all detected moisture source regions to precipitation can be found in Appendix A: Supplementary Material.

3.2. Climatological analysis of precipitation

In order to describe the global characteristics of precipitation, MSWEP annual (Fig. 2) and monthly (Fig. 3) climatological precipitation means are presented at a global scale. As anticipated, the annual distribution of precipitation shows highest values in the tropical and subtropical zones located between 0° and 20° north and south, located over areas of South America, Central South Africa, South Asia (India, Thailand, Cambodia), Indonesia, and Papa New Guinea. Areas further north such as the West Coast of Canada, Central Europe, and Norway also have among the highest precipitation, with 4 mm/day or more. The lowest values are observed in semi-arid and arid regions of Africa, the coast

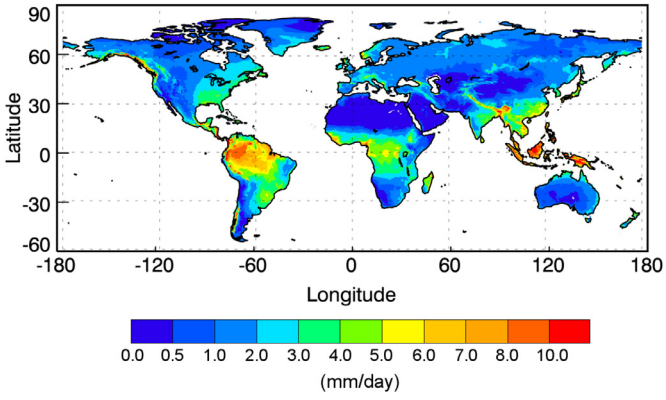

Fig. 2. Annual climatological precipitation values (1980–2015) from the Multi-Source Weighted-Ensemble Precipitation database (MSWEP). (For interpretation of the references to color in this figure, the reader is referred to the web version of this article.)

of the Middle East, Central parts of Asia, and Australia, with less than 0.3 mm/day. Moderate precipitation, between 1.5 and 2.5 mm/day, are mostly recorded over Europe, West Russia, and the eastern United States and Canada. The general distribution of precipitation from the MSWEP database is similar to other climatological precipitation datasets, such

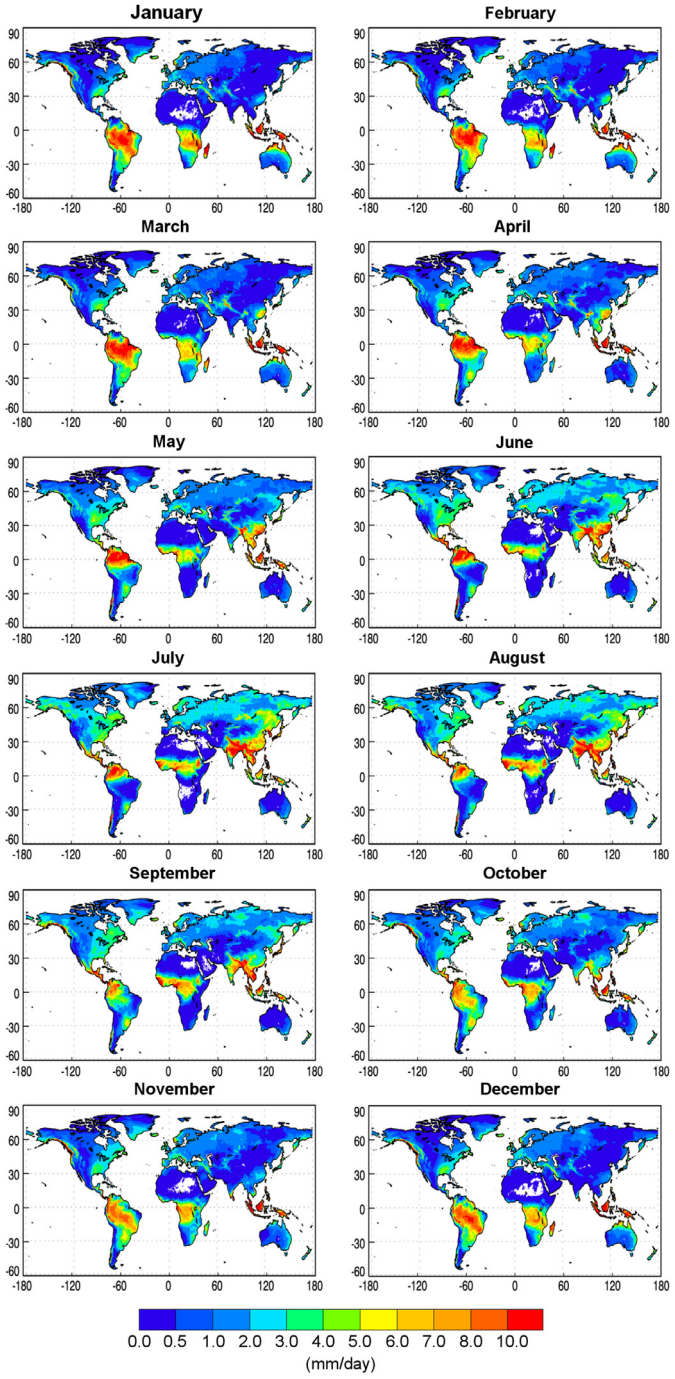

Fig. 3. Monthly precipitation climatology (1980–2015) from the Multi-Source Weighted-Ensemble Precipitation database (MSWEP). (For interpretation of the references to color in this figure, the reader is referred to the web version of this article.)

as the Global Precipitation Climatology Project (GPCP) (Huffman et al., 1997) and ERA-Interim (Simmons et al., 2007; Sun et al., 2018).

3.3. Contribution from the major moisture sources to extreme precipitation in the Peak Precipitation Month (PPM)

3.3.1. PPM identification

The climatological (1980–2015) monthly precipitation data from MSWEP is used to detect the month that exhibits the maximum precipitation (Fig. 4a) for each grid point, namely the Peak Precipitation Month (PPM). The PPM varies significantly between regions. From the results in Fig. 4a, it can be seen that the movement of the Inter Tropical Convergence Zone (ITCZ) towards the warmer hemisphere (Xian and Miller, 2008) causes PPMs in December to February (austral summer) around latitudes from 10°S to 30°S over central parts of South America and South Africa, and northern Australia. During July and August (boreal summer) this occurs over southern Asia, the Sahel, and Central Africa, and between the band 5° - 30°N in America.

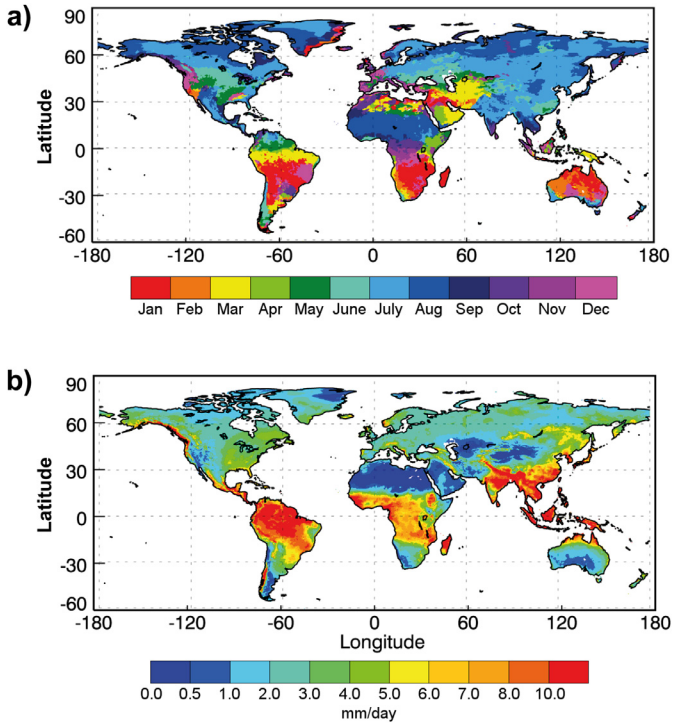

Fig. 4. (a) Peak Precipitation Month (PPM) based on monthly MSWEP data, and (b) monthly precipitation values associated with the PPM using MSWEP data (PMSWEP). (For interpretation of the references to color in this figure, the reader is referred to the web version of this article.)

Further north, and across most of the Asian continent, northern Europe, and northern and central North America, PPMs occur between June and August. March predominates as the PPM over the eastern Middle East and the band from 1°S–10°S over South America. It is interesting to note that for the Mediterranean and central North America, the pattern is the most diverse. The PPMs along the European Atlantic coast occur during boreal winter months, which is the period with the most active precipitation, associated with storm tracks; this is also the case for the Pacific coast of North America.

Fig. 4b shows the monthly precipitation during the PPM using MSWEP data (PMSWEP). The areas around the equator, which are affected by the ITCZ show the highest precipitation, with more than 8 mm/day. This is twice the mean annual values (4–5 mm/day, see Fig. 2). On the other hand, arid or semiarid regions in Africa, the Middle East, central Asia, or Australia receive the least precipitation (less than 1 mm/day) during the PPMs. In summary, for most areas worldwide, the PPM value of precipitation is double the mean annual value.

3.3.2. Characterization of preferred moisture source and its contribution to extreme precipitation

Having defined the PPM for every grid point, it is highly relevant to investigate the proportions of the contributions of the main global moisture sources for this extreme precipitation month. For this purpose, the total moisture contributions from all the sources (PFLEX) considered and the source that provides the greatest contribution (hereinafter denoted the Preferred Source (PS)) is considered. The PS associated with

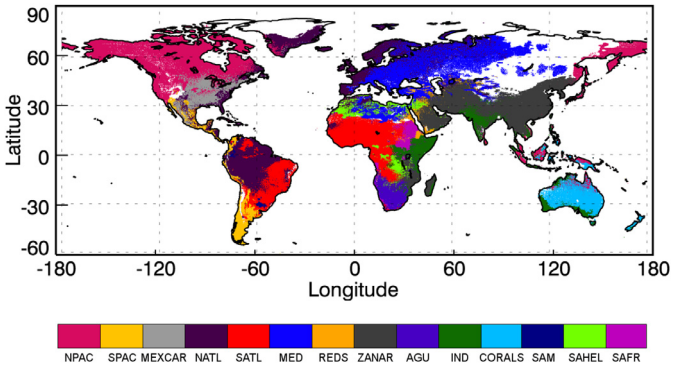

Fig. 5. Preferred sources of moisture for precipitation during the peak precipitation month for each location. (For interpretation of the references to color in this figure, the reader is referred to the web version of this article.)

the PPM at each grid point is shown in Fig. 5. The map shows that for the European Atlantic coast, from the Iberian to the Scandinavian Peninsula, the preferred moisture source is NATL (North Atlantic Ocean). For Northern Europe to Eurasia, and for North Africa, the preferred source of moisture is MED (the Mediterranean Sea). For most of Australia, the PS is the Coral Sea. For the southern cone of South America and for Central America, SPAC contributes the most precipitation during the PPM. While NATL is the PS over the Amazon River Basin, SATL (South Atlantic Ocean) prevails over most of eastern South America and Central Africa. On the other hand, for South Africa the PS is AGU (Agulhas Current). The NPAC (North Pacific) dominates in Alaska, Canada, and the northern United States, which also extends its influence to some parts of Russia. The MEXCAR (Mexico Caribbean) is the PS for the eastern cone of the United States and some parts of Mexico. It is interesting to note that in Central and East Asia, including the Middle Eastern coast, the detected preferred source is ZANAR (Zanzibar Current and Arabian Sea). As expected, IND (Indian Ocean) dominates in India and extends its influence over eastern Africa.

The moisture contribution from the PS in the PPM (PS-PFLEX) is shown in Fig. 6a, and the contributions associated with all the detected moisture sources can be observed in Fig. A.13a in the Supplementary Material. In order to provide a better understanding of how Fig. A.13a was created, an example is presented below. For each grid point the values where E-P < 0 are added together for all the detected sources for each PPM. For instance, for North America the PPM is July and the moisture for precipitation is supported only by a single source, namely the NPAC (North Pacific) (see Fig. 1, for July). Thus, the precipitation values calculated from FLEXPART (E-P<0) in Fig. 6a for that region are only those associated with NPAC moisture source. On the other hand, there are regions where two or more moisture sources contribute to precipitation during the PPM. This is the case over the South Arabian Peninsula, Iraq, Iran and Kazakhstan regions where the PPM is March (see Fig. 4a in yellow), and the precipitation in March (see the Figure in the Supplementary Material) is supported by moisture from REDS (Red Sea) and ZANAR (Zanzibar Current and Arabian Sea). Therefore, in these cases and for each grid point, the contributions of both sources are added together.

The general pattern shown in both figures (Fig. 6a and A.13a) is similar to that shown in Fig. 4b. However, the difference in magnitude reflects the fact that only the major moisture sources (represented in Figs. 1 and A.1–12 in the Supplementary Material) from FLEXPART outputs are considered (only a single source (the PS) for Fig. 6a, and all the major sources for Fig. A.13a in the Supplementary Material); Fig. 4b shows the total precipitation using MSWEP data. The missing moisture is made up from the remaining oceanic and continental evaporative areas that are not included as major sources.

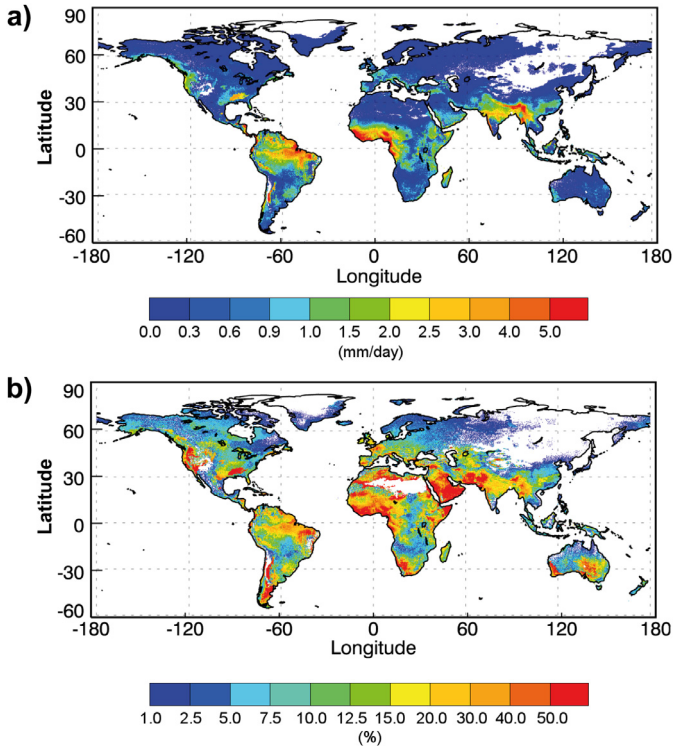

Fig. 6. (a) Gridded precipitation contribution during peak precipitation months (PPM) identified via Lagrangian experiments associated with only the Preferred Moisture Source (PS-PFLEX). (b) Contributed percentage by the PS-PFLEX to the monthly precipitation values during the PPM using MSWEP data (PMSWEP). (For interpretation of the references to color in this figure, the reader is referred to the web version of this article.)

In order to assess the importance of the primary source in each case, Fig. 6b shows the ratio of the precipitation from the PS (Fig. 6a) to the precipitation (PMSWEP, Fig. 4b) in the PPM (the same for Fig. A.13b in the Supplementary material but rating PFLEX from all the major moisture sources and PMSWEP). It is important to stress that for the calculation of the ratio, PMSWEP values of less than 0.1 mm/day are not considered. In general, there are no important differences between the ratio associated with all the sources (Fig. A.13b in Supplementary materials) and that associated only with the PS (Fig. 6b). This suggests that the contribution of the PS is generally much greater than the remaining main moisture sources affecting each region. The lower ratios of precipitation for the PPM explained by the PS (and the main global moisture sources in general) occur at higher latitudes over the northern hemisphere. However, more than 50% of the precipitation is explained by the main moisture sources over most of Africa, southern Asia and eastern Brazil, or southern Argentina (Fig. 6b). These results suggest that the main global moisture sources have a higher impact and relevance on precipitation over lower latitudes. Over higher latitudes, however, extreme precipitation seems to have a different origin and/or that there is a higher number of sources affecting the extreme precipitation patterns.

Summary and conclusions

In this work a detailed global analysis of climatological and extreme precipitation (in terms of the PPM) is performed; and the identification, variability and relative contribution of the main oceanic and continental sources to these precipitation patterns is also investigated. The moisture sources detected in this work are similar to those found by Gimeno et al. (2010) and Castillo et al. (2014). Most of the detected sources are oceanic and located over tropical and subtropical areas; only

some regions over Africa and South America appear as continental moisture sources. In general terms, the sources show important variability in their extent and contribution throughout the year.

For extreme precipitation these results reflect important geographical differences. For the PPM, summer months show higher precipitation over most of the Asian continent, northern Europe, northern and central North America, southern Africa and most of South America and Australia; however, the PPM along the European Atlantic coast occurs during boreal winter, which is in agreement with most studies on extreme precipitation (Catto and Pfahl, 2013; Lavers and Villarini, 2013; Hénin et al., 2019).

The impact of the PS on the precipitation amount in the PPM varies geographically. Despite, for example, NPAC and MED sources are over vast areas in norther hemisphere, the percentage of their contribution to extreme precipitation is, in general, low. On the other hand, other sources of moisture such as ZANAR or SATL provide over 50% of precipitation occurring during the PPM. From our results, the moisture contribution associated with the PS does not show important differences compared with the case where all the main moisture sources are taken into consideration.

The contributions from the major global oceanic sources should provide most of the moisture for precipitation at a global scale, nevertheless in regional terms there are some specific areas for which the main moisture sources are not necessary located over the most evaporative areas. From results presented in this paper it can be addressed that the moisture contribution from the major sources strongly resembles the precipitation pattern of observed global precipitation, in terms of both climatological and extreme precipitation.

The analysis presented here is also useful for further applications, such as the analysis of the influence of moisture transport according to the major modes of variability (as ENSO, PNA or NAO) over the preferred sources during the peak precipitation month, and the role of particular local synoptic conditions, as well the relationship between climate change and the occurrence of extreme events, such as floods or droughts, is well known. Since understanding moisture transport from the main global sources towards continental areas provides valuable data for investigating these events, the information presented in this study could be very useful for further studies of climate change.

The study of possible changes over time of both PPM or/and PS could be of great interest. Changes in the behaviour of moisture transport, in terms of quantity, from the preferred sources could affect the intensity and/or frequency of extreme precipitation events. Moreover, focus for further investigation would be possible changes in PPM over the last few decades, to verify whether the potential changes are due to modification in the PS moisture contribution to precipitation. This signal could be another valuable indicator of regional or global climate change.

Finally, it should be noted that since this assessment is performed using monthly data, results obtained for specific daily extreme precipitation events may have different contributions (in preferred moisture sources and/or its percentage). This daily analysis will be addressed in future research for individual synoptic situations.

Funding

This work forms part of the LAGRIMA project. Danica Ciric is supported by the European Commission under the Erasmus Mundus Project Green-Tech-WB: Smart and Green Technologies for Innovative and Sustainable Societies in the Western Balkans (551,984-EM-1–2014–1-ES-ERA Mundus-EMA2). Marta Vazquez is supported by the Xunta de Galicia under grant ED481B 2018/062. Margarida L.R. Liberato acknowledges funding from Fundação para a Ciência e a Tecnologia, Portugal (FCT) and Portugal Horizon 2020 through project WEx-Atlantic (PTDC/CTA-MET/29,233/2017). This work was partially supported by Xunta de Galicia under Project ED431C 2017/64-GRC “Programa de Consolidación e Estructuración de Unidades de Investigación Competitivas (Grupos de Referencia Competitiva)”.

Supplementary material

Supplementary material associated with this article can be found, in the online version, at doi:10.1016/j.advwatres.2019.103385.

References

Beck, H.E., van Dijk, A.I.J.M., Levizzani, V., Schellekens, J., Miralles, D.G., Martens, B., de Roo, A., 2017. MSWEP: 3-hourly 0.25° global gridded precipitation (1979–2015) by merging gauge, satellite, and reanalysis data. Hydrol. Earth Syst. Sci. 21, 589–615. https://doi.org/10.5194/hess-21-589-2017.

Butt, N., Seabrook, L., Maron, M., Law, B.S., Dawson, T.P., Syktus, J., McAlpine, C.A., 2015. Cascading effects of climate extremes on vertebrate fauna through changes to low-latitude tree flowering and fruiting phenology. Glob. Change Biol. 21, 3267–3277. https://doi.org/10.1111/gcb.12869.

Castillo, R., Nieto, R., Drumond, A., Gimeno, L., 2014. The role of the ENSO cycle in the modulation of moisture transport from major oceanic moisture sources. Water Resour. Res. 50, 1046–1058. https://doi.org/10.1002/2013WR013900.

Catto, J.L., Pfahl, S., 2013. The importance of fronts for extreme precipitation. J. Geophys. Res.Atmosph. 118, 10791–10801. https://doi.org/10.1002/jgrd.50852.

Ciric, D., Stojanovic, M., Drumond, A., Nieto, R., Gimeno, L., 2016. Tracking the origin of moisture over the Danube river basin using a lagrangian approach. Atmosphere (Basel) 7, 162. https://doi.org/10.3390/atmos7120162.

Dee, D., Uppala, S.M., Simmons, A.J., Berrisford, P., Poli, P., Kobayashi, S., Andrae, U., Balmaseda, M.A., Balsamo, G., Bauer, P., Bechtold, P., Beljaars, A.C.M., van de Berg, L., Bidlot, J., Bormann, N., Delson, C., Dragani, R., Fuentes, M., Geer, A.J., Haimberger, L., Healy, S.B., Hersbach, H., Hólm, E.V., Isaksen, L., Kallberg, P., Köhler, M., Matricardi, M., McNally, A.P., Monge-Sanz, B.M., Morcrette, J.J., Park, B.K., Peubey, C., de Rosnay, P., Tavolato, C., Thépaut, J.N., Vitar, F., 2011. The ERA interim reanalysis: configuration and performance of the data assimilation system. Quart. J. R. Meteorol. Soc. 137, 553–597. https://doi.org/10.1002/qj.828.

Drumond, A., Marengo, J., Ambrizzi, T., Nieto, R., Moreira, L., Gimeno, L., 2014. The role of Amazon Basin moisture on the atmospheric branch of the hydrological cycle: a Lagrangian analysis. Hydrol. Earth Syst. Sci. 18, 2577–2598. https://doi.org/10.5194/hessd-18-2577-2598.

Drumond, A., Nieto, R., Gimeno, L., Ambrizzi, T., 2008. A Lagrangian identification of major sources of moisture over central Brazil and La Plata basin. J. Geophys. Res. 113, D14128. https://doi.org/10.1029/2007JD009547.

Fischer, E.M., Beyerle, U., Knutti, R., 2013. Robust spatially aggregated projections of climate extremes. Nat. Clim. Chang 3, 1033–1038. https://doi.org/10.1038/nclimate2051.

Frank, D., Reichstein, M., Bahn, M., Thonicke, K., Frank, D., Mahecha, M.D., Smith, P., Velde, M., Vicca, S., Babst, F., Beer, C., Buchmann, N., Canadell, J.G., Ciais, P., Cramer, W., Ibrom, A., Miglietta, F., Poulter, B., Rammig, A., Seneviratne, S.I., Walz, A., Wattenbach, M., Zavala, M.A., Zscheischler, J., 2015. Effects of climate extremes on the terrestrial carbon cycle: concepts, processes and potential future impacts. Glob. Change Biol. 21, 2861–2880. https://doi.org/10.1111/gcb.12916.

Gimeno, L., Drumond, A., Nieto, R., Trigo, R.M., Stohl, A., 2010. On the origin of continental precipitation. Geophys. Res. Lett. 37, L13804. https://doi.org/10.1029/2010GL043712.

Gimeno, L., Nieto, R., Drumond, A., Castillo, R., Trigo, R., 2013. Influence of the intensification of the major oceanic moisture sources on continental precipitation. Geophys. Res. Lett. 40, 1443–1450. https://doi.org/10.1002/grl.50338.

Gimeno, L., Stohl, A., Trigo, R.M., Dominguez, F., Yoshimura, K., Yu, L., Drumond, A., Durán-Quesada, A.M., Nieto, R., 2012. Oceanic and terrestrial sources of continental precipitation. Rev. Geophys. 50, RG4003. https://doi.org/10.1029/2012RG000389.

Hénin, R., Ramos, A.M., Schemm, S., Gouveia, C.M., Liberato, M.L.R., 2019. Assigning precipitation to mid-latitudes fronts on sub-daily scales in the north Atlantic and european sector: climatology and trends. Int. J. Climatol. 39, 317–330. https://doi.org/10.1002/joc.5808.

Heydarizad, M., Raeisi, E., Sori, R., Gimeno, L., 2018. The identification of Iran’s moisture sources using a Lagrangian particle dispersion model. Atmosphere (Basel) 9, 408. https://doi.org/10.3390/atmos9100408.

Hoerling, M., Eischeid, J., Perlwitz, J., Quan, X.W., Wolter, K., Cheng, L., 2016. Characterizing recent trends in U.S. heavy precipitation. J. Clim 29, 2313–2332. https://doi.org/10.1175/JCLI-D-15-0441.1.

Huffman, G.J., Adler, R.F., Arkin, P., Chang, A., Ferraro, R., Gruber, A., Janowiak, J., McNab, A., Rudolf, B., Schneider, U., 1997. The global precipitation climatology project (GPCP) combined precipitation dataset. Bull. Am. Meteorol. Soc. 78, 5–20. https://doi.org/10.1175/1520-0477(1997)078<0005:TGPCPG>2.0.CO;2.

Knapp, A.K., Hoover, D.L., Wilcox, K.R., Avolio, M.L., Koerner, S.E., La Pierre, K.J., Loik, M.E., Luo, Y., Sala, O.E., Smith, M.D., 2015. Characterizing differences in precipitation regimes of extreme wet and dry years: implications for climate change experiments. Glob. Change Biol. 21, 2624–2633 . https://doi.org/10.1111/gcb.12888.

Lavers, D.A., Villarini, G., 2013. The nexus between atmospheric rivers and extreme precipitation across Europe. Geophys. Res. Lett. 40, 3259–3264. https://doi.org/10.1002/grl.50636.

Nieto, R., Gimeno, L., 2019. A database of optimal integration times for Lagrangian studies of atmospheric moisture sources and sinks. Sci. Data 6 (59), 1–10. https://doi.org/10.1038/s41597-019-0068-8.

Nieto, R., Gimeno, L., Drumond, A., Hernandez, E., 2010. A Lagrangian identification of the main moisture sources and sinks affecting the mediterranean area. WSEAS Trans. Environ. Devel. 5, 365–374 ISSN: 1790-5079.

Nolet, P., Kneeshaw, D., 2018. Extreme events and subtle ecological effects: lessons from a long-term sugar maple–American beech comparison. Ecosphere 9 (7). https://doi.org/10.1002/ecs2.2336.

Numaguti, A., 1999. Origin and recycling processes of precipitating water over the Eurasian continent: Experiments using an atmospheric general circulation model. J. Geophys. Res. 104, 1957–1972. https://doi.org/10.1029/1998jd200026.

O'Lenick, C.R., Wilhelmi, O.V., Michael, R., Hayden, M.H., Baniassadi, A., Wiedinmyer, C., Monaghan, A., Crank, P.J., Sailor, D.J., 2019. Urban heat and air pollution: a framework for integrating population vulnerability and indoor exposure in health risk analyses. Sci. Total Environ. 0048–9697. https://doi.org/10.1016/j.scitotenv.2019.01.002.

Ramos, A.M., Tomé, R., Trigo, R.M., Liberato, M.L.R., Pinto, J.G., 2016. Projected changes in atmospheric rivers affecting Europe in CMIP5 models. Geophys. Res. Lett. 43, 9315–9323. https://doi.org/10.1002/2016GL070634.

Santos, C., Costa, A., 2014. Recent changes in temperature and precipitation extremes in an ecological reserve in Federal District, Brazil. Revista Brasileira de Meteorol. 29 (1), 13–20. https://doi.org/10.1590/S0102-77862014000100002.

Sato, T., Tsujimura, M., Yamanaka, T., Iwasaki, H., Sugimoto, A., Sugita, M., Kimura, F., Davaa, G., Oyunbaatar, D., 2007. Water sources in semiarid northeast asia as revealed by field observations and isotope transport model. J. Geophys. Res. 112, D17112. https://doi.org/10.1029/2006JD008321.

Simmons, A., Uppala, S., Dee, D., Kobayashi, S., 2007. ERA-Interim: new ECMWF reanalysis products from 1989 onwards. ECMWF Newslett. 110, 25–35. https://doi.org/10.21957/pocnex23c6.

Singh, D., Tsiang, M., Rajaratnam, B., Diffenbaugh, N.S., 2013. Precipitation extremes over the continental United States in a transient, high-resolution, ensemble climate model experiment. J. Geophys. Res. Atmosph. 118, 7063–7086. https://doi.org/10.1002/jgrd.50543.

Smith, M.D., 2011. The ecological role of climate extremes: current understanding and future prospects. J. Ecol. 99, 651–655. https://doi.org/10.1111/j.1365-2745.2011.01833.x.

Sodemann, H., Zubler, E., 2010. Seasonal and inter-annual variability of the moisture sources for Alpine precipitation during 1995–2002. Int. J. Climatol. 30, 947–961. https://doi.org/10.1002/joc.1932.

Sodemann, H., Schwierz, C., Wernli, H., 2008. Interannual variability of Greenland winter precipitation sources: Lagrangian moisture diagnostic and north Atlantic oscillation influence. J. Geophys. Res. 113, D03107. https://doi.org/10.1029/2007JD008503.

Sorí, R., Nieto, R., Vicente-Serrano, S.M., Drumond, A., Gimeno, L., 2017. A Lagrangian perspective of the hydrological cycle in the Congo river basin. Earth Syst. Dynam 8, 653–675. https://doi.org/10.5194/esd-8-653-2017.

Stohl, A., 1999. The Flexpart particle dispersion model version 3.1. User Guide. University of Munich, Germany Available online https://folk.nilu.no/~andreas/flexpart/flexpart31.pdf.

Stohl, A., James, P., 2005. A lagrangian analysis of the atmospheric branch of the global water cycle: part II: moisture transports between Earth's ocean basins and river catchments. J. Hydrometeorol. 6, 961–984. https://doi.org/10.1175/JHM470.1.

Stohl, A., James, P., 2004. A lagrangian analysis of the atmospheric branch of the global water cycle. Part I: method description, validation, and demonstration for the august 2002 flooding in central Europe. J. Hydrometeorol. 5, 656–678. https://doi.org/10.1175/1525-7541(2004)005<0656:ALAOTA>2.0.CO;2.

Stohl, A., Forster, C., Frank, A., Seibert, P., Wotawa, G., 2005. Technical note: the Lagrangian particle dispersion model FLEXPART version 6.2. Atmos. Chem. Phys. 5, 2461–2474. https://doi.org/10.5194/acp-5-2461-2005.

Sun, Q., Miao, C., Duan, Q., Ashouri, H., Sorooshian, S., Hsu, K.L., 2018. A review of global precipitation data sets: data sources, estimation, and inter-comparisons. Rev. Geophys. 56, 79–107. https://doi.org/10.1002/2017RG000574.

Tandon, N.F., Zhang, X., Sobel, A.H., 2018. Understanding the dynamics of future changes in extreme precipitation intensity. Geophys. Res. Lett. 45, 2870–2878. https://doi.org/10.1002/2017GL076361.

Toreti, A., Desiato, F., 2008. Changes in temperature extremes over Italy in the last 44 years. Int. J. Climatol. 28, 733–745. https://doi.org/10.1002/joc.1576.

Trenberth, K.E., 2011. Changes in precipitation with climate change. Clim. Res. 47, 123–138. https://doi.org/10.3354/cr00953.

van der Ent, R.J., Savenije, H.H.G., 2013. Oceanic sources of continental precipitation and the correlation with sea surface temperature. Water Resour. Res. 49, 3993–4004. https://doi.org/10.1002/wrcr.20296.

van der Ent, R.J., Savenije, H.H.G., Schaefli, B., Steele-Dunne, S.C., 2010. Origin and fate of atmospheric moisture over continents. Water Resour. Res. 46, W09525. https://doi.org/10.1029/2010WR009127.

Van der Ent, R.J., Tuinenburg, O.A., 2017. The residence time of water in the atmosphere revisited. Hydrol. Earth Syst. Sci. 21, 779–790. https://doi.org/10.5194/hess-21-779-2017.

Vázquez, M., Nieto, R., Drumond, A., Gimeno, L., 2016. Moisture transport into the Arctic: source-receptor relationships and the roles of atmospheric circulation and evaporation. J. Geophys. Res. Atmosph. 121. https://doi.org/10.1002/2016JD02540.

Westra, S., Alexander, L.V., Zwiers, F.W., 2013. Global increasing trends in annual maximum daily precipitation. J. Clim. 26, 3904–3918. https://doi.org/10.1175/JCLI-D-12-00502.1.

Xian, P., Miller, R.L., 2008. Abrupt seasonal migration of the ITCZ into the summer hemisphere. J. Atmos. Sci. 65, 1878–1895. https://doi.org/10.1175/2007JAS2367.1.

Xue, T., Tang, G., Sun, L., Wu, Y., Liu, Y., Dou, Y., 2017. Long-term trends in precipitation and precipitation extremes and underlying mechanisms in the U.S. great basin during 1951–2013. J. Geophys. Res. Atmosph. 122, 6152–6169. https://doi.org/10.1002/2017JD026682.